POSTER: Geometric modeling of pelvic organs with a discrete offset approach

Thierry Bay
Aix-Marseille University,
LSIS UMR CNRS 7296,
Avenue Escadrille
Normandie-Niemen, 13397
Marseille, FRANCE
thierry.bay@lsis.org

Romain Raffin
Aix-Marseille University,
LSIS UMR CNRS 7296,
Avenue Escadrille
Normandie-Niemen, 13397
Marseille, FRANCE
romain.raffin@lsis.org

Marc Daniel
Aix-Marseille University,
LSIS UMR CNRS 7296,
Avenue Escadrille
Normandie-Niemen, 13397
Marseille, FRANCE
marc.daniel@lsis.org

ABSTRACT

In order to design a patient-specific simulator of pelvic organs, MoDyPe project considers the organs as thick surfaces. Starting from a closed parametric surface for the outer hull, an offset approach is applied. However, respecting the thickness on the surface and ensuring the absence of self-intersection is impossible if the shape has too important local curvatures. Two iterative approaches are compared. The first method is based on a B-spline formulation, and the second one on a mass-spring system (MSS). Our second method on discrete representation permits to obtain more accurate results with a more flexible formulation of the problem.

Keywords: Offset approach, parametric fitting, B-spline, mass-spring system.

1 INTRODUCTION

Through simulations of organs, a better understanding of poorly known disorders is possible. The problem we are interested in refers to the pelvic area, whose the organs can suffer from an imbalance in their spatial configuration. Although surgery is used to heal the patient, the impact of a surgical operation is difficult to estimate. Many tools have been developed for this purpose, requiring a virtualization of the environment [ZG12].

This work is integrated into a preoperative and patient-specific process (described in [BCR+11]) to develop a decision support software. The invasive procedures to displace the organs will be evaluated. The real-time constraint is relaxed to be faithful to physiological reality. From MRI of patients, a segmentation is carried out, followed by a geometric modeling to get meshes and a physical modeling to simulate the organs behavior. The geometric modeling is based on physiological reality by considering thick surfaces, i.e. a volume mesh with an internal cavity. But the MRI datasets can be poor quality, so the inner boundary of the organs can not be segmented because of the noise and erroneous points. Therefore, starting from a B-spline describing the surface of the organs [BCR+12], a volume mesh is created

with an offset approach by building a second surface at a given distance from the first one (the thickness of the membrane, alias the offset-distance).

Firstly, related work is detailed and offset problems are put forward, followed by a brief description of the offset process with B-spline surfaces. Afterwards, a discrete formulation of the problem is presented. A qualitative comparison is carried out between the results obtained by a B-spline offset and the discrete offset.

2 RELATED WORK

In our case, the creation of an offset consists in providing a thick membrane composed of hexahedra without degenerate or crossed elements to apply finite element calculations. The known problem of parametric offsets is the local and global intersections when the minimal main curvature is too large according to the offset-distance (cf. Figure 1). The problem is clearly considered in the literature (cf. [KN02] about the parametric offsets): removing the loops by working on each line and column [KSP02] for ordered datasets, curvature reduction by an iterative repositioning of the control points [SNL04], or parametric restriction [SEK06]. Finally these methods may not detect small self-intersections.

In another point of view, models based on active contours could be used [YPH+06]. The parameterization of a B-spline surface makes it possible to control easily the sampling, so that a quality conform mesh is created. However, the advantage of active contours is to make a seed evolve with a set of forces, without taking into consideration the connections with the external mesh. Their drawback in our process comes from automatic
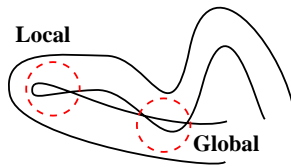
Figure 1: Local and global intersections for a curve.

feedbacks of the physical step that requires modifications in the surface sampling (i.e. local density change). These needs involve an expensive update of the mesh connections with the internal non-parameterized mesh to ensure the absence of crossed hexahedron.

3 THICKNESS AND B-SPLINE

Based on [BCR+12], a bidirectional energy function describes the connections between the B-spline sampling and the data points. The error is defined as a sum of distances between each sampled point with the closest data point in terms of Euclidean distance, and vice versa. A steepest descent method is used to reduce this energy and a fitting surface can be found.

3.1 Offset Operator and Process

From the surface fitted on the data of a patient (called *external surface*), the construction of an *offset-surface* at an *offset-distance* consists of four steps: uniform discretization of the external surface, computation of the normal at each point of its sampling, construction of the *offset-cloud* by moving each sampled point along the normal over the value of the *offset-distance*, and iterative fitting of a parametric closed surface on the *offset-cloud* to obtain the *offset-surface*. If several layers are needed by FEM experts to have a mesh with more uniform hexahedra, the same process is repeated with the value of the thickness divided by the number of layers.

3.2 Results

The cardinalities of the datasets are around 40K points. Since the real thicknesses are unknown, average values are used [SSS+10]: 3.5 mm for the bladder, 5.5 mm for the rectum. Uterus and vagina are not considered.

Figure 2(a) illustrates the bladder membrane. The offset does not have any problems because the shape is quite spherical, besides the thickness is not enough important to create global self-intersections. The histogram in Figure 2(b) sums up the errors during the process for each layer and the value of the local thickness to reach. The errors are the two energy functions [BCR+11] and the maximum error during the fitting. We notice that the maximum error for each new layer is low compared to the *offset-distance*. The results are different for the rectum. Figure 3(a) shows local self-intersections due to high curvature. Figure 3(b) illustrates effectively the problem of the maximum error between two layers.
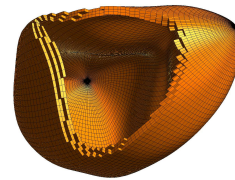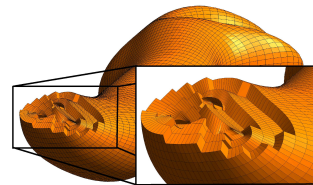

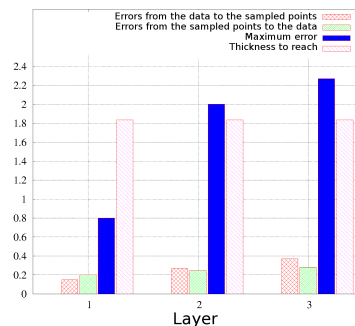(a) Thickness with 3 layers
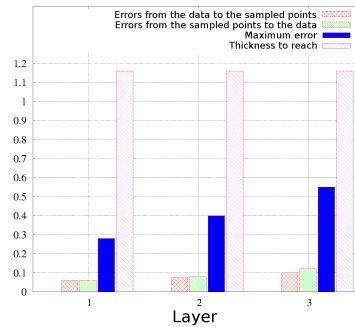
(b) Mean squared and maximum errors (mm)

Figure 2: Offset of a bladder wall.

(a) Self-intersections

(b) Mean squared and maximum errors (mm)

Figure 3: Offset of a rectum.

3.3 Assets and Limitations

For organs without complex shapes, the preceding method is satisfactory. The scattered knowledge on the real patient-specific thicknesses remains a problem. However, the use of a method based on the least squares has limitations. One of the solution is to apply a trimming algorithm as described in Section 2, nevertheless the parametric methods are unadapted especially for large *offset-distances*. Since we provide a mesh in output, working directly on the mesh would be an advantage. We have then developed a discrete approach for the offset construction based on a mass-spring system (MSS).

4 THICKNESS AND MSS

A MSS is designed to build the internal surface without accurate knowledge about the thicknesses. We differentiate our model from conventional mechanical approaches, since our objective is to use a dynamic approach to create a static mesh. In our case, no mass is considered. A set of $(n+1) \times (m+1)$ particles $\{P_{i,j}\}_{i,j=0}^{n,m}$ forms the system (the external surface sampling). Each one has a position $p_{i,j}$, a velocity $\dot{p}_{i,j}$ and an acceleration $\ddot{p}_{i,j}$ at a given time t. The system is governed by Newton's second law of motion $F_{i,j} = \ddot{p}_{i,j}$, with $F_{i,j}$ the sum of all forces at $P_{i,j}$.

4.1 Creation of the Thickness

The choice of the lattice requires to define the field of application and the constraints to satisfy.

4.1.1 Energies of the System

An external force F_{ext} (oriented as the normal vector at each $P_{i,j}$) and a damping force F_{damp} (based on Kelvin-Voigt model) are added to the system. Finally, Hooke's law is used as part of internal force for elasticity and distances preservation:

$$F_{stretch}(P_{i,j}) = \sum_{k,l} k_{ij,kl} \left((p_{k,l} - p_{i,j}) - L_{ij,kl}^0 \right) \frac{p_{k,l} - p_{i,j}}{\|p_{k,l} - p_{i,j}\|} \quad (1)$$

where $k_{ij,kl}$ is the stiffness coefficient linking $P_{i,j}$ and $P_{k,l}$ if they are neighboring, and $L_{ij,kl}^0$ is the rest length of the spring. Two springs are however added to constraint the internal mesh in an orthogonal position inside (cf. Figure 4). The total internal force consists of:

$$F_{int}(P_{i,j}) = F_{stretch}(P_{i,j})$$
$$+ \hat{k}_{i,j} \left(\|S(u_i, v_j) - p_{i,j}\| - \hat{L}_{i,j}^0 \right) \frac{S(u_i, v_j) - p_{i,j}}{\|S(u_i, v_j) - p_{i,j}\|}$$
$$+ \tilde{k}_{i,j} \left(\|p_{i,j}^\perp - p_{i,j}\| - \tilde{L}_{i,j}^0 \right) \frac{p_{i,j}^\perp - p_{i,j}}{\|p_{i,j}^\perp - p_{i,j}\|}$$
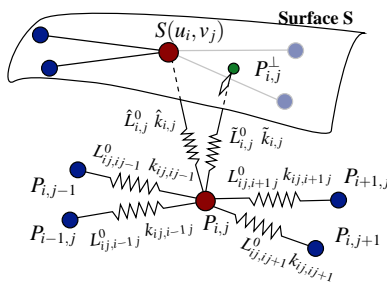$$(2)$$

Figure 4: Lattice of the system.

4.1.2 Integration Scheme

The total force of the system applied on $P_{i,j}$ at time t is:

$$F_{tot}(P_{i,j}, t) = F_{int}(P_{i,j}, t) + F_{damp}(P_{i,j}, t) + F_{ext}(P_{i,j}, t) \quad (3)$$

The Euler explicit scheme is sufficient to compute the next position of $P_{i,j}$ with small time steps:

$$\begin{cases} \ddot{p}_{i,j}(t + \Delta t) = F_{tot}(P_{i,j}, t) \\ \dot{p}_{i,j}(t + \Delta t) = \dot{p}_{i,j}(t) + \Delta t \, \ddot{p}_{i,j}(t + \Delta t) \\ p_{i,j}(t + \Delta t) = p_{i,j}(t) + \Delta t \, \dot{p}_{i,j}(t + \Delta t) \end{cases} \quad (4)$$

with Δt the fixed time step, whose the value must not exceed the natural period of the system [Pro96].

4.2 Parameters of the MSS

If we take into account the time step Δt, we end up with a set of $12(n+1) \times (m+1) + 3$ parameters for the MSS. Determination of the optimal values of each parameter would be too much time-consuming and empirical.

Tests of local self-intersections are performed during the iterations, increasing these stiffness values settings if necessary. Similarly, the rest length $L_{ij,kl}^0$ is replaced by L_{ij}^0. This length is defined initially through simulations, by increasing gradually the tension force until the OBB of the internal mesh has only 10% of its initial volume (fixed threshold). Concerning the parameters of the two additional springs in the lattice, the rest lengths are equals to the *offset-distance*, then $\hat{L}_{i,j}^0 = d$ and $\tilde{L}_{i,j}^0 = d$. From an isotropic assumption for the external force, we set $\hat{k}_{i,j} = \tilde{k}_{i,j} = K$, with K the unique stiffness coefficient connecting the internal and external meshes. Finally, the parameters γ, η and Δt are determined empirically, since the associated forces are difficult to match with physical quantities.

4.3 Correction of Local Self-Intersections

A local self-intersection is defined as an inversion of a quadrangle in the internal mesh. Our proposed solution consists in detected the crossed quadrangles and to increase locally the mesh tension with the stiffness parameters (their values do not go beyond a precalculated threshold to prevent instability in the system). The detection is achieved with oriented angles (see Figure 5). Moreover, this tension is spread on the 2-neighborhood, with a geometric decrease q^e (with q the proportion between two stiffness values, and e the depth of the neighborhood for the considered particle).
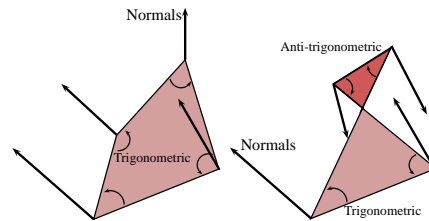
(a) Well-oriented angles (b) Crossed quadrangle

Figure 5: Oriented angles of crossed quadrangles.

4.4 Results

The input of the process is the external surface sampling (coarse for the visualization). Figure 6(a) illustrates the use of the total force for a rectum, building the internal mesh within the form. To improve the tests with the constitutive laws, the hexahedral mesh should be nearly uniform (they should look like as much as possible to cubes). Since the thickness is not neglected, several layers are generated by linear interpolation between the two layers (see Figure 6(b)).

(a) Application of the total force
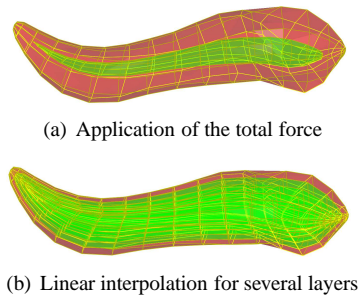

(b) Linear interpolation for several layers

Figure 6: Construction of a rectum.

Tables 1 and 2 show a comparison between the discrete and parametric approach to construct the rectum thickness. For the parametric approach, we note that half as many cells have reached the expected thickness. In addition, the minimum value highlights the problem of proximity between the layers in some areas. With the discrete approach, the maximum is higher than with the B-spline. The *offset-distance* is indeed locally superior in the MSS to ensure stability with the internal force. A rate of 25% of elements remain to achieve, but the couple *tension/orthogonal force* is difficult to manage.

	Min.	Max.	Mean	St. dev.
B-spline	0.0004	6.4	3.89	1.96
MSS	2.3	11.6	6	1.77

Table 1: Analysis of the rectum thickness (in mm).

	> 5.5 mm (%)	> 90% of 5.5 mm (%)
B-spline	24.7 %	52 %
MSS	55.5 %	73 %

Table 2: Rectal wall thicknesses beyond 90% and 100% of the *offset-distance*.

4.5 Assets

The thickness management is handled by the combined action of external and internal forces. Local self-intersections are avoided by increasing the weight of the quadrangular tension on the mesh. Moreover, many of the system parameters can be estimated.

5 CONCLUSION

The parametric approach based on the least squares offers advantages for fitting problems. Obviously, in case of high curvature of the surface, a proper offset can not be built. Our method allows us to have a direct control over the forces and corrects the local self-intersections. It is not based on a priori knowledge (corpus, skeleton) and is performant in noisy data environments (due to approximation and tension management). Results are validated by medical experts on experimental data. The hexahedral resulting mesh can be defined by FEM experts in terms of points density or number of layers.

Concerning the future works, a good asset would be to detect the global intersections. However the empirical dimension remains difficult to manage. A purely geometric orientation will therefore be investigated.

6 ACKNOWLEDGEMENTS

7 REFERENCES

[BCR+11] T. Bay, J.-C. Chambelland, R. Raffin, M. Daniel, and M.-E. Bellemare. Geometric modeling of pelvic organs. In IEEE, editor, *33rd Annual International Conference of the IEEE Engineering in Medicine and Biology Society*, pages 4329–4332, Boston, USA, 2011.

[BCR+12] T. Bay, Z.-W. Chen, R. Raffin, M. Daniel, P. Joli, Z.-Q. Feng, and M.-E. Bellemare. Geometric modeling of pelvic organs with thickness. In Atilla M. Baskurt and Robert Sitnik, editors, *Three-Dimensional Image Processing (3DIP) and Applications II*, volume 8290, pages 82900I–1–82900I–14, Burlingame, USA, 2012.

[KN02] M. A. Kulczycka and L. J. Nachman. Qualitative and quantitative comparisons of B-spline offset surface approximation methods. In *CAD*, volume 34, pages 19–26, 2002.

[KSP02] G. V. V. Ravi Kumar, K. G. Shastry, and B. G. Prakash. Computing non-self-intersecting offsets of NURBS surfaces. In *CAD*, volume 34, pages 209 – 228, 2002.

[Pro96] X. Provot. Deformation constraints in a mass-spring model to describe rigid cloth behavior. In *Graphics Interface*, pages 147–154, 1996.

[SEK06] J.-K. Seong, G. Elber, and M.-S. Kim. Trimming local and global self-intersections in offset curves/surfaces using distance maps. In *CAD*, volume 38, pages 183–193. Butterworth-Heinemann, 2006.

[SNL04] Y. F. Sun, A. Y. C. Nee, and K. S. Lee. Modifying freeformed NURBS curves and surfaces for offsetting without local self-intersection. In *CAD*, volume 36, pages 1161–1169, 2004.

[SSS+10] M. Schuenke, E. Schulte, U. Schumacher, L.M. Ross, E.D. Lamperti, M.M. Voll, and K.H. Wesker. *Neck and Internal Organs*, volume 20, chapter 2. Thieme, 2010.

[YPH+06] P.A. Yushkevich, J. Piven, H.C. Hazlett, R. Gimpel Smith, S. Ho, J.C. Gee, and G. Gerig. User-guided 3D active contour segmentation of anatomical structures: Significantly improved efficiency and reliability. In *NeuroImage*, volume 31, pages 1116 – 1128, 2006.

[ZG12] Bo Zhu and Lixu Gu. A hybrid deformable model for real-time surgical simulation. In *Computerized Medical Imaging and Graphics*, volume 36, pages 356 – 365, 2012.